Desalination and Water Treatment
www.deswater.com
doi: 10.1080/19443994.2015.1069218

57 (2016) 15164–15175
July

Taylor & Francis
Taylor & Francis Group

Molecularly imprinted polymers (MIPs): a functional material for removal of humic acid from peat water

M.A. Zulfikar[a,*], D. Wahyuningrum[b], R.R. Mukti[c], H. Setiyanto[a]

[a]*Analytical Chemistry Research Group, Institut Teknologi Bandung, Jl. Ganesha 10, Bandung 40132, Indonesia, emails: zulfikar@chem.itb.ac.id (M.A. Zulfikar), henry@chem.itb.ac.id (H. Setiyanto)*
[b]*Organic Chemistry Research Group, Institut Teknologi Bandung, Jl. Ganesha 10, Bandung 40132, Indonesia, email: deana@chem.itb.ac.id*
[c]*Physical and Inorganic Chemistry Research Group, Institut Teknologi Bandung, Jl. Ganesha 10, Bandung 40132, Indonesia, email: rino@chem.itb.ac.id*

Received 9 November 2014; Accepted 30 June 2015

ABSTRACT

The aim of this study is to investigate the use of moleculary imprinted polymers (MIPs) material as an alternative adsorbent for the adsorption of humic acid (HA) from peat water in batch mode. The MIPs were prepared with methyl methacrylate as a monomer, HA as templates, ethylene glycoldimethacrylate as a cross-linker, and dimethyl formamide as a solvent. The characteristics of MIPs were evaluated using Fourier transform infra-red spectroscopy, scanning electron microscope, and Brunauer–Emmett–Teller methods. The Langmuir, Freundlich, and Sips models were applied to describe the equilibrium isotherms using non-linear regression analysis. Pseudo-first-order, pseudo-second-order, intraparticles, and Boyd kinetic models were used to describe the kinetic data. The results showed that the equilibrium contact time was 60 min. The experimental results indicated that the percentage of sorption increases with an increase in the adsorbent dosage and temperature. The adsorption percentage decreased with increasing peat water pH from 2 to 12. The equilibrium data fitted well for the Langmuir adsorption isotherms, with monolayer adsorption capacity of MIPs found to be 45.45 mg/g. The results of the kinetic study show that the adsorption of HA onto MIPs could be described by the pseudo-second-order kinetic model with a rate constant in the range of 0.034–0.115 g/mg min and controlled by film diffusion, with the effective diffusion coefficient was found in the range of 7.42×10^{-8}–13.84×10^{-8} cm^2/s. Thermodynamic parameters data indicated that under the experimental conditions, the HA adsorption process was non-spontaneous and endothermic, with the Gibbs free energy (ΔG°) in the range of 3.71–1.17 kJ/mol, whereas enthalpy (ΔH°) and entropy (ΔS°) at 16.17 and 42.70 J mol^{-1}, respectively.

Keywords: Adsorption; Humic acid; Isotherm; MIPs; Peat water

*Corresponding author.

1. Introduction

Humic acid (HA) is one of the major components of peat water which is formed by the microbial degradation of biomolecules. The presence of HA in water may lead to yellowish or brownish color, taste and odor problems, and to biological instability of drinking water in distribution systems. Moreover, the high affinity of humic substances for complexation with various pollutants including heavy metals and pesticides could cause contamination of ground and surface water. In addition, during chlorination step in drinking water treatment, HA will form very toxic disinfection by-products (chlorinated organic compounds including trihalomethanes) which exhibit mutagenic properties. Thus, the removal of HA from surface water or wastewater is very important.

Different methods have been applied for removal of HA. These include coagulation–flocculation [1–4], electro-coagulation [5], oxidation [6], photocatalysis [7], biofiltration [8], and membrane technology [4,9–11]. However, these methods are not widely used due to their high costs and economic disadvantages. Due to their simplicity and high efficiency, adsorption treatments have been extensively applied to remove organic pollutants in aqueous environments. In the past years, several adsorbents have been employed for HA adsorption including activated carbon [12–14], eggshell [15], bentonite [16–19], chitin and chitosan [20–24], silica [25], fly ash [26–28], metal hydroxide [29], and others [30–34].

Molecularly imprinted polymers (MIPs) are synthetic materials having artificially generated recognition sites able to rebind a specific target molecule. These materials are obtained by polymerizing functional and cross-linking monomers around a template molecule, leading to a highly cross-linked, three-dimensional network polymer. The monomers are chosen by considering their ability to interact with the functional groups of the template molecule. Once polymerization has taken place, the template molecule is extracted to establish binding sites with shape, size, and functionalities complementary to the target analyte. The resulting MIPs are stable, and they show many advantages such as high mechanical strength, robustness, and resistance to a wide range of pH, solvents, and temperatures. Therefore, their use for the treatment of complex matrices, environmental samples, or food and beverage samples has rapidly become widespread [35–37].

In the present work, a selective MIP intended to adsorption of HA from peat water was prepared. The MIPs and the correspondent non-imprinted polymers (NIPs) were prepared by radical polymerization technique. The physical properties of the MIPs were characterized by Fourier transform infra-red (FT-IR) spectroscopy, scanning electron microscope (SEM), zeta potential, and Brunauer–Emmett–Teller (BET) method. The effects of agitation time, pH, adsorbent dosage, and temperature on adsorption of HA from peat water were investigated. The kinetics of the removal process were determined using pseudo-first-order, pseudo-second-order, intraparticle diffusion, and Boyd kinetic models. The Langmuir, Freundlich, and Sips isotherm models were used to evaluate the equilibrium adsorption data.

2. Materials and methods

2.1. Materials

Methyl methacrylate (MMA) as a functional monomer, HA as a template, ethylene glycoldimethacrylate (EGDMA) as a cross-linker, 2,2-azo bis isobutyronitrile (AIBN) as an initiator, and dimethyl formamide (DMF) as a solvent were purchased from Merck (USA). All chemicals used were analytical grade and without further purification.

Peat water sample was obtained from Rimbo Panjang, a subdistrict of Kampar in Riau Province, Indonesia. The characteristics of peat water sample can be seen in Table 1.

2.2. MIPs material preparation

The MIPs material synthesis was proposed by blending of 5 mmol of MMA (0.500 g), 20 mmol of EGDMA (4.20 g), and 100 mg of AIBN to HA as a template. This solution was stirred for about 30 min until a homogeneous solution was attained. The prepared solution was then cooled to 0℃, purged with nitrogen (99.99%) for 10 min, sealed, and heated at 60℃ during 24-h stirring. The obtained materials were grounded in a mortar and dried in a hot air oven at

Table 1
The characteristic of peat water sample

Parameters	Unit	Result
Color	Pt–Co	522
Organic compounds	mg/L $KMnO_4$	276
pH	–	4.02
Conductivity	μS/cm	82
Turbidity	mg/L SiO_2	7.8
Iron	mg/L	0.32
Manganese	mg/L	0.15
Calcium	mg/L	0
Magnesium	mg/L	6.7

60˚C for 2 h and sieved to acquire the powdered particles. The machine was set to automatically sieve the grinded sample at a particle size of 75 μm. ca. Five grams of these powdered particles were subjected to leaching with 200 mL of 5 M HNO_3 for 5 h to obtain MIPs material, and then washed with methanol. After washing, the sorbent particles were dried by means of vacuum, after which they were ready for use. The control polymer materials, i.e. the NIPs, were prepared in a similar way to that of the MIPs preparation, but without the HA molecule as a template.

2.3. Characterization of MIPs material

FT-IR spectroscopy was used to identify the chemical groups present in the MIPs. The samples were examined using a Perkin Elmer 3100 spectrophotometer within the range of 400–4,000 cm^{-1}. The relation seeds/KBr employed was approximately 1% in weight. The background obtained from the scan of the air (without sample in the spectrophotometer window) was automatically subtracted from the sample spectra. The surface morphologies of the MIPs and NIPs materials were analyzed using a SEM (JEM-2010, JEOL). The surface area of MIPs was analyzed through nitrogen adsorption measurements at 77 K using Micromeritics Gemini 2370 (USA) equipment.

2.4. Batch sorption studies

Each 0.5 g of the MIPs and NIPs materials were placed in a 100 mL Erlenmeyer flask containing 50 mL of peat water sample. The mixtures were stirred in thermostatic shaker bath (Innova 3000, 3000) at 100 rpm and at 25˚C for 1, 5, 10, 20, 30, 40, 60, 90, 120, and 240 min. After that, the suspension was taken out and the supernatant was centrifugated. The supernatant was then analyzed for the remaining HA concentration by an ultraviolet-visible spectrophotometer model UV–vis 1601 (Shimadzu, Japan) at the λ 400 nm [23]. The percent adsorption of HA was calculated using the following equation:

$$\%\ \text{Adsorption} = \frac{C_i - C_e}{C_i} \times 100 \quad (1)$$

where C_i and C_e are the initial and final concentrations of HA (mg/L) in solution, respectively.

The adsorption capacity of an adsorbent was obtained from the mass balance on the sorbate in a system with solution volume V, which is expressed as:

$$q_e(\text{mg/g}) = \frac{C_i - C_e}{m} \times V \quad (2)$$

where C_i and C_e are the initial and final concentrations of HA (mg/L) in solution, respectively. V is the volume of solution (L) and m is the mass of materials (g) used.

The effects of adsorbent dosage on HA adsorption from peat water were investigated by agitating different dosages of MIPs particles (0.05; 0.1; 0.25; 0.5; 0.75; and 1 g) in 50 mL peat water for 60 min at original pH of peat water (= 4.02) and shaking speed at 100 rpm.

The dependence of HA adsorption on pH was studied through batch sorption experiments in the pH range from 2 to 12, by shaking a series of bottles containing 0.5 g of MIPs and 50 mL peat water solution in a thermostatic shaker bath for 60 min and shaking speed at 100 rpm. The pH was adjusted by addition of 0.1 M HCl and NaOH.

The effect of temperature on HA adsorption was determined by shaking 0.5 g of MIPs in 50 mL peat water at four different temperatures 25, 45, 65, and 80˚C at original pH of peat water and shaking speed at 100 rpm.

2.5. Study of adsorption isotherm

The HA adsorption isotherm experiments using MIPs materials were conducted by mixing 0.5 g of MIPs with 50 mL peat water, with other conditions were held constant at contact time of 60 min, temperature of 25˚C, and at original pH of peat water. The experimental data were then calculated to determine the adsorption isotherm by using the Langmuir, Freundlich, and Sips models.

2.6. Study of adsorption kinetics

The HA removal kinetics study was performed by mixing 0.5 g of MIPs with 50 ml of peat water sample at temperature of 25, 45, 65, and 80˚C for 1, 5, 10, 20, 30, 40, 60, 90, 120, and 240 min, with other conditions were held constant at pH of 4.12, particle size of 75 μm, and shaking speed at 100 rpm. The experimental data were then calculated to determine the adsorption kinetics using the pseudo-first-order, pseudo-second-order, intraparticle, and Boyd kinetic models.

3. Results and discussion

3.1. Characterization of MIPs adsorbent particles

The FT-IR spectra of the MIPs after removing the template as well as the NIPs, all prepared under the optimal conditions, are presented in Fig. 1. It can be

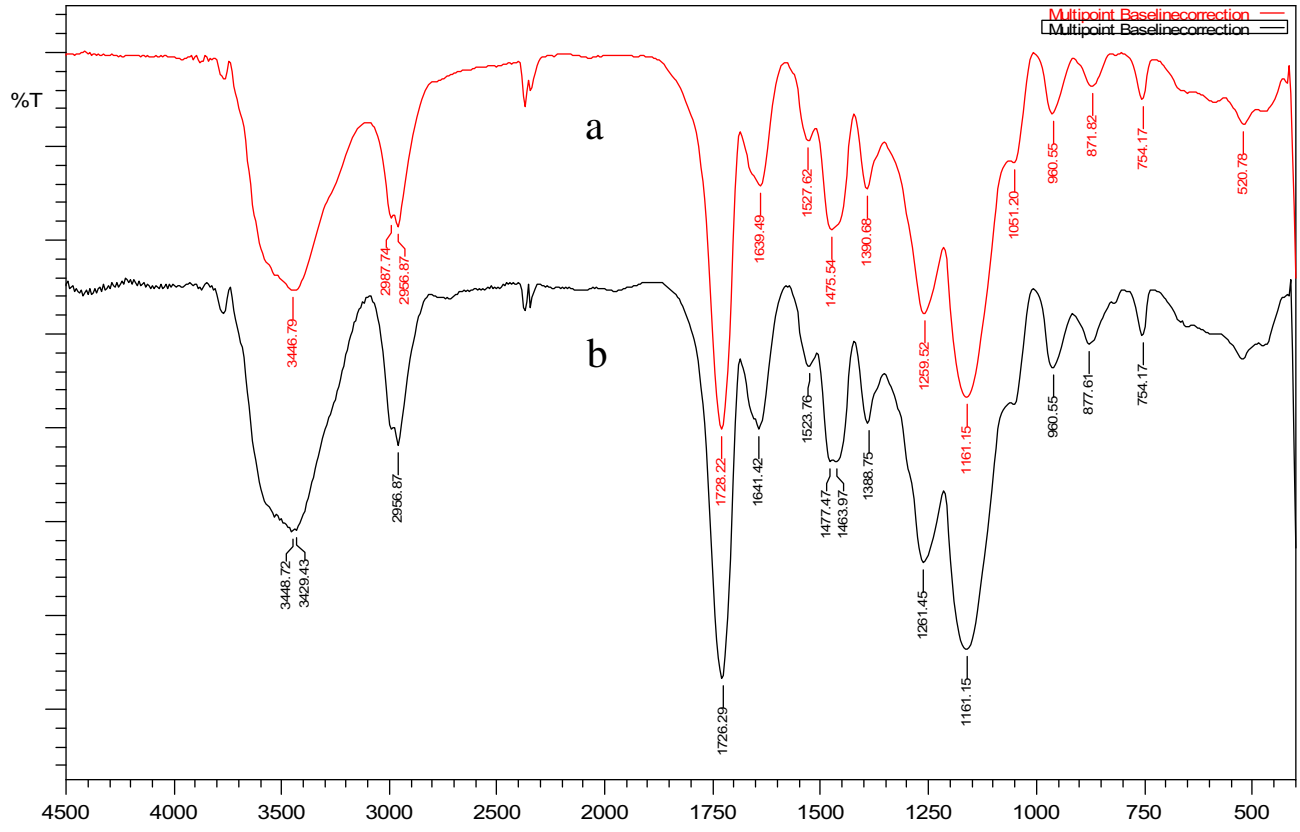

Fig. 1. FT-IR spectrum of (a) NIPs and (b) MIPs materials.

seen from Fig. 1(a) that the NIPs exhibited a stretching vibration band of –CH at a wavelength of 2,956.87 cm^{-1}. The peak at 1,728.22 cm^{-1} was assigned to stretching vibration band of C=O, while the peaks at 1,475.54 and 1,161.15 cm^{-1} were assigned to the stretching vibration bands of $–CH_3$ and $–O–CH_3$, respectively. One surprising observation was that there was no significant difference between MIPs and NIPs spectrum and the absorption bands corresponding to the HA were not observed in the MIPs spectra (Fig. 1(b)), which demonstrates that HA molecules were washed off during the leaching process.

From the two photos (Fig. 2(a) and (b)), we can know that the surface of MIPs was rougher than that of NIPs and there were many cavities in MIPs but few in NIPs, which indicated that MIPs had many imprinting cavities that were favorable for rebinding template molecules while NIPs had not. Thereby, the MIPs had stronger adsorption capacity to the template than the NIPs did.

Fig. 3 shows the N_2 adsorption–desorption isotherms for the MIPs with its corresponding control adsorbent particles (the NIPs). Detail characteristics of the pore structure of the imprinted and non-imprinted polymers prepared are presented in Table 2. It is worth noting that the BET surface area did not change significantly between the imprinted polymer and the control polymer. This result precluded the assumption that the porous features of the polymers are not dependent on the imprinted template. Similar results have been reported by Gómez–Pineda et al. [38].

3.2. Effect of agitation time on adsorption processes

The effect of agitation time on HA adsorption onto the MIPs and the NIPs materials is shown in Fig. 4. It can be seen that for both the adsorbent materials, a rapid initial adsorption of HA takes place at the beginning of agitation time and thereafter, the adsorption increases gradually with an increase in the agitation time and reaches equilibrium after 60 min. This may be due to the high availability in the number of vacant surface sites at the initial stage.

From Fig. 4, we can also observe that the amount of HA adsorption using the MIPs is higher than that of using the NIPs for the same agitation time period. This result demonstrated the excellent imprinting effect of the MIPs materials adsorbent for the HA.

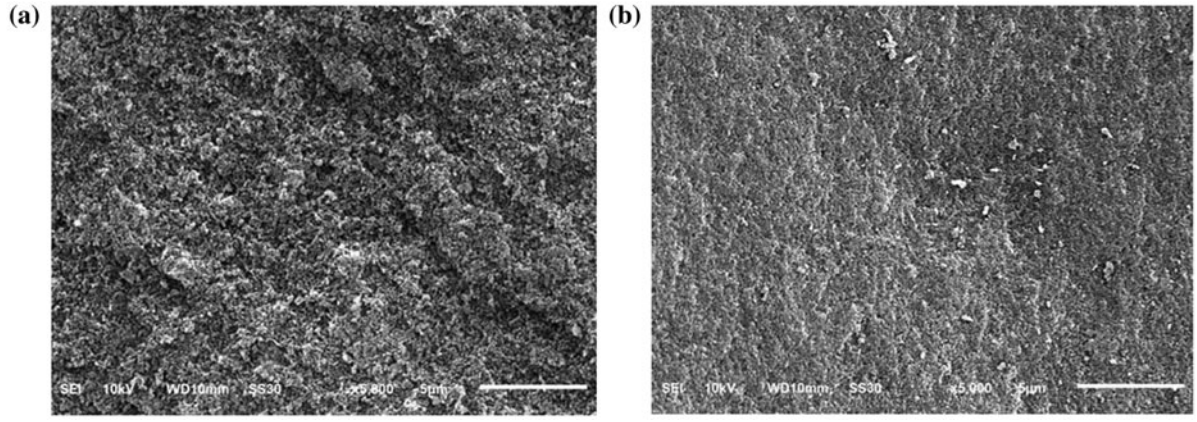

Fig. 2. Surface morphology of (a) MIPs and (b) NIPs materials.

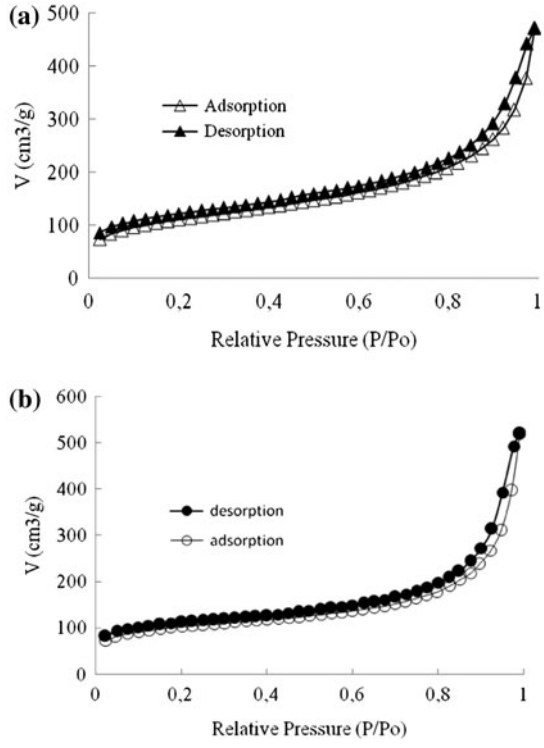

Fig. 3. N_2 adsorption–desorption isotherm for (a) MIPs and (b) NIPs materials.

Table 2
Characteristics of MIPs and NIPs adsorbent particles

Parameters	MIPs	NIPs
BET surface area (m^2/g)[a]	381	343
Micro pore volume (cm^3/g)[b]	0.03	0.06
Total pore volume (cm^3/g)	0.7	0.8

[a]Applying BJH model.
[b]Determined by *t*-plot.

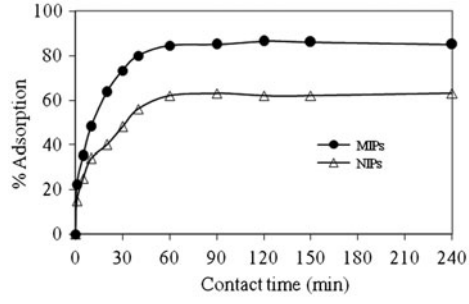

Fig. 4. Effect of agitation time on HA removal from peat water (volume 50 mL, dosage 0.5 g, pH 4.02, particle size 75 μm, shaking speed 100 rpm, and temp. 25°C).

3.3. Effect of dosage on adsorption processes

Adsorbent dosage is an important parameter because it determines the capacity of an adsorbent for a given initial concentration of the adsorbate [39,40]. To investigate the adsorption capacity of the MIPs, different amounts of particles adsorbent ranging from 0.05 to 1.0 g were mixed with the peat water for 60 min. The amount of HA removed by adsorption using the MIPs are presented in Fig. 5. It is observed that, the percentage removal of the HA increases with an increase in the dosages until a point where any further addition of adsorbent did not cause any significant change in the percentage of adsorption. Increased HA adsorption with increasing MIPs dosage is attributed to the increase of total adsorbent surface area. Near optimum adsorption was observed in the case of 0.5 g of MIPs.

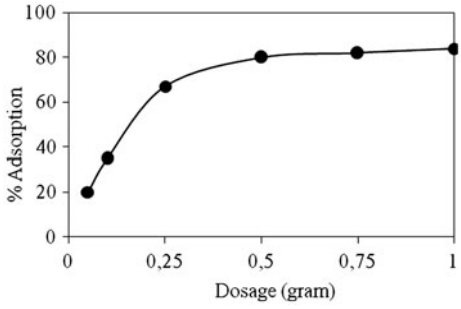

Fig. 5. Effect of adsorbent dosage on HA removal from peat water (contact time: 60 min, volume 50 mL, pH 4.02, particle size 75 μm, shaking speed 100 rpm, and temp. 25°C).

3.4. Effect of pH on removal processes

To explore the effects of solution pH of the peat water on the percentage removal of HA, a series of solutions with pH values from 2.0 to 12 was prepared. The experiment was carried out at 25°C and the results are shown in Fig. 6. As shown in Fig. 6, the experimental data showed that the adsorption was higher in acidic conditions than in basic ones; the higher HA adsorption was achieved at pH 2. With increasing pH value, the HA adsorption was shown to diminish. This indicates that the adsorption of HA from peat water using the MIPs is favored at lower pH values. It was stated that the MIPs contain polar functional groups such as carboxylic group in their molecular structure, which can be involved in adsorption. At low pH, the concentration of H^+ ion in the system increases and this functional group was protonated, with the surface of the adsorbent acquiring a positive charge. As previously explained, HA is the main component of peat water, which consists of many phenolic and carboxylic functional groups, and can be ionized in aqueous medium and may acquire a negative charge. Hence, in acidic conditions, these groups are led to the imprinted cavities of the MIPs due to the strong electrostatic forces from the protonated carboxylic groups of the MIPs, or other possible driving forces such as van der Waals' and hydrophobic interactions.

With the increase of peat water pH, less polar functional groups on the MIPs surface were protonated and the adsorbent became more negatively charged; thus, the electrostatic repulsion between the these functional groups and adsorbent occurred, which leads to a decrease in the amount of HA adsorption.

3.5. Effect of temperature on adsorption processes

The effects of temperature on the adsorption of HA using MIP materials are shown in Fig. 7. As shown in Fig. 7, the adsorption capacity of the HA increased with increasing temperature. This is due to increase in the mobility of HA molecule with increasing temperature [13,18,26] where more molecules move across the external boundary layer and the internal pores of the adsorbent particles. Furthermore, increasing temperature may produce a swelling effect within the internal structure of adsorbent, making possible the penetration of the large HA molecule further [41–46]. Similar results have been reported on acid activated Greek bentonite [18], on unburnt carbon [26], on bentonite [17], as well as on activated carbon prepared from biomass material [13].

3.6. Adsorption isotherm

The adsorption isotherm represents the relationship between the amount adsorbed by a unit weight of solid adsorbent and the amount of adsorbate remained in the solution at the equilibrium time. In

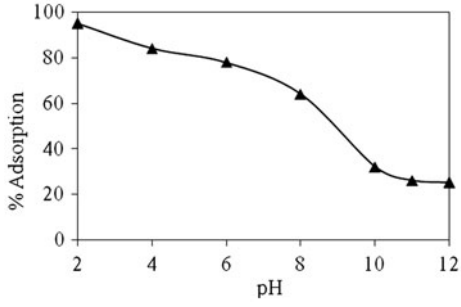

Fig. 6. Effect of pHs on HA removal from peat water (contact time: 60 min, volume 50 mL, dosage 0.5 g, particle size 75 μm, shaking speed 100 rpm, and temp. 25°C).

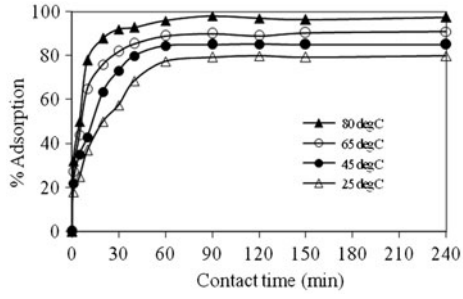

Fig. 7. Effect of temperatures on HA removal from peat water (volume 50 mL, dosage 0.5 g, pH 4.02, particle size 75 μm, and shaking speed 100 rpm).

this experiment, three equilibrium isotherm models of Langmuir, Freundlich, and Sips were examined. Langmuir isotherm refers to homogeneous adsorption, where adsorption can only occur at a fixed number of definite localized sites, with no transmigration of the adsorbate in the plane of the surface. The Langmuir model can be given as:

$$q_e = \frac{q_m b C_e}{1 + b C_e} \tag{3}$$

where C_e is the equilibrium concentration (mg/L), q_e is amount of adsorbate adsorbed per unit weight of absorbent (mg/g), q_m and b are the maximum adsorption capacity (mg/g), and Langmuir constant (L/mg), respectively.

The Freundlich isotherm model is derived by assuming a heterogeneous surface of adsorption capacity and adsorption intensity with a non-uniform distribution of heat of adsorption, in which it is characterized by the heterogeneity factor, $1/n$. The Freundlich equation can be written as:

$$q_e = K_f C_e^{1/n} \tag{4}$$

where C_e is the equilibrium concentration (mg/L), q_e is amount of adsorbate adsorbed per unit weight of absorbent (mg/g), and K_f and n are Freundlich constants. A value of $1/n$, ranging between 0 and 1, is a measure of adsorption intensity or surface heterogeneity. A value for n greater than one indicates of a favorable adsorption process. The other Freundlich constant K_f indicates the adsorption capacity of the adsorbent.

Sips isotherm is employed to analyze the equilibrium data obtained during batch adsorption studies. Sips model is a combination of the Langmuir and Freundlich models, having features of both the Langmuir and Freundlich equations. It is expressed as:

$$q_e = \frac{q_m K_{eq} C_e^n}{1 + K_{eq} C_e^n} \tag{5}$$

Sips isotherm equation is characterized by the heterogeneity factor, n, and it can be employed to describe the heterogeneous system. K_{eq} (L/mg) represents the equilibrium constant of Sips equation and q_m (mg/g) is the maximum adsorption capacity. When $n = 1$, Sips isotherm equation reduces to the Langmuir equation and it implies a homogeneous adsorption process [46].

Fig. 8 shows the fitting curves to the experimental data. The parameters of the three isotherms calculated based on Eqs. (3)–(5) by non-linear regression using

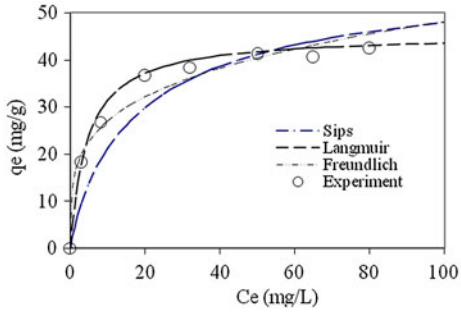

Fig. 8. Isotherm curve for HA removal from peat water (contact time: 60 min, volume 50 mL, pH 4.02, particle size 75 μm, shaking speed 100 rpm, and temp. 25°C).

Excel software are presented in Table 3. As shown in Fig. 8, the Langmuir isotherm model fits well to the experimental results more than the Freundlich and Sips isotherm models do, indicating that the adsorption of HA from peat water onto the MIPs is a monolayer adsorption. In addition, the isotherm parameters from the models indicate that the Langmuir isotherm produces a better fitting result in terms of regression coefficient (Table 3). Based on the Langmuir isotherm model, the maximum adsorption of HA from peat water onto the MIPs at pH 4.01 and 25°C is found to be 45.45 mg/g.

3.7. Adsorption kinetics

The kinetics of adsorption is vital because it controls the efficiency of the process. In this study, the pseudo-first-order, pseudo-second-order, intraparticle diffusion, and Boyd kinetic models were applied to investigate the controlling mechanisms of the adsorption of HA onto the MIPs materials. The pseudo-first-order equation can be expressed as Eq. (6):

$$log\,(q_e - q_t) = log\,q_e - (k_1/2.303)t \tag{6}$$

The pseudo-second-order model is based on the assumption of chemisorption of the adsorbate on the adsorbents. This model is given as Eq. (7):

$$t/q_t = 1/k_2 q_e^2 + t/q_e \tag{7}$$

where q_t is the amount of adsorption of HA (mg/g) at time t (min), and k_1 (min^{-1}), k_2 (g/mg/min) are the adsorption rate constant of pseudo-first-order and pseudo-second-order adsorption, respectively. The validity of the two models can be interpreted by the linear plots of log $(q_e - q_t)$ vs. t and (t/q_t) vs. t,

Table 3
Langmuir, Freundlich, and Sips constants for HA adsorption

Langmuir model			Freundlich model			Sips model			
b (L/mg)	q_m (mg/g)	R^2	n	K_f (mg/g)	R^2	q_m (mg/g)	K_{eq} (mL/g)	n	R^2
0.224	45.45	0.994	4.00	15.21	0.967	45.82	0.098	0.858	0.988

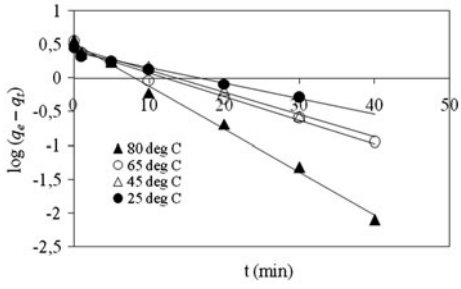

Fig. 9. Pseudo-first-order model plots for HA removal from peat water at different temperatures (volume 50 mL, dosage 0.5 g, pH 4.02, particle size 75 μm, and shaking speed 100 rpm).

respectively. The rate constants k_1 and k_2 can be obtained from the plot of experimental data.

Fig. 9 shows the kinetics of HA adsorption by using pseudo-first-order model, and its kinetics parameters are shown in Table 4. It was observed that the pseudo-first-order kinetic model does not adequately fit the experimental values. Also from Table 4, it is indicated that the values of the correlation coefficients are not high for the various temperatures solution. Furthermore, a large difference of equilibrium adsorption capacity (q_e) between the experiment and calculation was observed, indicating a poor pseudo-first-order fit to the experimental data.

Plot of t/q_t against t for pseudo-second-order model under different temperatures are shown in Fig. 10. From the slope and intercept values, q_2 and k_2 were calculated and the results are shown in Table 4. The linear plots of t/q_t vs. t show a good agreement with experimental data giving the correlation coefficients close to 1. Also, the calculated q_2 values agree very well with the experimental data at all temperature. This means that the adsorption kinetics of HA onto the MIPs obeys the pseudo-second-order kinetic model for the entire adsorption period.

Adsorption kinetics is usually controlled by different mechanisms, and the most general of which is the diffusion mechanism. To investigate the mechanism of adsorption, the intraparticle diffusion and Boyd kinetic models is used. The intraparticle diffusion model can be defined as:

$$q_t = k_d t^{1/2} + C \tag{8}$$

where k_d and C are an intraparticle diffusion rate constant (mg/g min$^{1/2}$) and a constant, respectively. The k_d is obtained from the slope of linier plot of q_t vs. $t^{1/2}$. If the plot of q_t vs. $t^{1/2}$ gives a straight line and passed through the origin, the sorption process is controlled by pore diffusion only. However, if the data exhibit multilinear plots, then two or more steps influence the sorption process.

From the plot of q_t against $t^{1/2}$ (Fig. 11), it can be seen that these plots generally have a dual nature, implying that more than one process affected the sorption. From these figure, it is clear that at all temperatures, the adsorption processes of the HA follows two phases, suggesting that the intraparticle diffusion (or pore diffusion) is not the rate-limiting step for the entire reaction. The initial portion of the plot indicated an external mass transfer (or film diffusion) whereas the second linear portion is due to intraparticle or pore diffusion. Extrapolating the linear portion of the

Table 4
The pseudo-first order and second-order kinetic parameters for HA adsorption from peat water using MIPs

	Pseudo-first-order			Pseudo-second-order			
Temperature (°C)	k_1 (min^{-1})	$q_{e,cal}$ (mg/g)	R^2	k_2 (min^{-1})	$q_{e,cal}$ (mg/g)	R^2	$q_{e,exp}$ (mg/g)
25	0.053	2.415	0.980	0.034	3.401	0.992	3.28
45	0.076	2.864	0.986	0.053	3.559	0.996	3.45
65	0.081	2.710	0.983	0.086	3.690	0.999	3.65
80	0.145	3.304	0.994	0.115	3.953	0.999	3.92

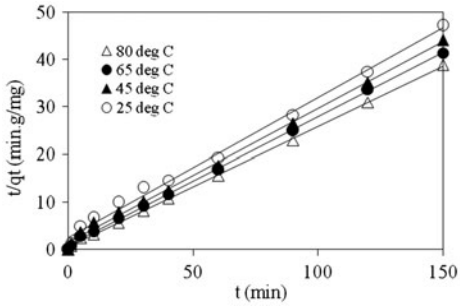

Fig. 10. Pseudo-second-order model plots for HA removal from peat water at different temperatures (volume 50 mL, dosage 0.5 g, pH 4.02, particle size 75 μm, and shaking speed 100 rpm).

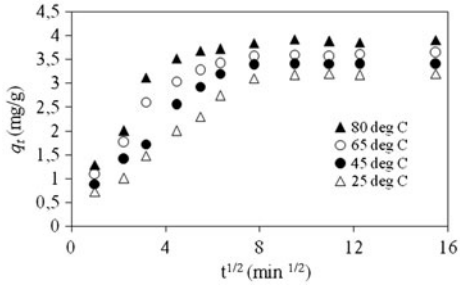

Fig. 11. Intraparticle model plot for HA removal from peat water at different temperatures (volume 50 mL, dosage 0.5 g, pH 4.02, particle size 75 μm, and shaking speed 100 rpm).

plot to the ordinate produces the intercept (C) which is proportional to the extent of boundary layer thickness [15,31,34,41,45–47]. The values of k_{d1} and k_{d2} as obtained from the slopes of the two straight lines are listed in Table 5.

The values of k_{d1} and k_{d2} for the adsorption of HA slightly increased with increasing temperature from 25 to 80°C. This indicated that increasing temperature slightly increases the migration of HA into the inner structure of the MIPs. From Table 5, we also can see that the value of C increased with increasing temperature.

Table 5
Parameter of the intraparticle diffusion model for the HA adsorption from peat water using MIPs

Temperature (°C)	k_{d1}	C_1	k_{d2}	C_2
25	0.371	0.292	0.001	3.153
45	0.453	0.398	0.003	3.375
65	0.504	0.701	0.009	3.485
80	0.561	0.883	0.014	3.700

This suggests that the effect of boundary layer diffusion for the adsorption of HA on the MIPs probably become more important at higher temperature because of the greater random motion associated with the increased thermal energy [34].

In order to determine the actual rate-controlling step involved in the HA adsorption process, the kinetic data as obtained by the batch method were further analyzed using the Boyd kinetics model. Boyd's kinetic model determines whether the main resistance to mass transfer is in the thin film (boundary layer) surrounding the adsorbent particle, or in the resistance to diffusion inside the pores. This model is expressed as:

$$B_t = -0.4977 - \ln(1 - F) \tag{9}$$

where B_t is a mathematical function of F, and F is the fraction of solute adsorbed at different times, t (h), which is calculated as follows:

$$F = q_t/q_\alpha \tag{10}$$

where q_α represents the amount sorbed (mg/g) at infinite time. The linearity of the plot of B_t vs. time is used to distinguish whether external (film diffusion) and intraparticle diffusion controls the adsorption rate [45,47–49].

A straight line passing through the origin is indicative of sorption processes governed by particle-diffusion (or pore diffusion) mechanisms. Otherwise they are governed by film diffusion or chemical reaction [48]. The calculated B values are used to calculate the effective diffusion coefficient, D_i (cm^2/s) from the equation:

$$B = \pi^2 D_i/r^2 \tag{11}$$

where r represents the radius of the sorbent particle (cm) by assumsing as spherical particles. From the plot of B_t against t (Fig. 12), it was observed that the plots are linear with high correlation coefficient at all temperatures but does not pass through origin, confirming that film diffusion is the rate-limiting step [48].

The calculated D_i values at different temperatures are provided in Table 6. If film diffusion is the rate-determining step, then the value of D_i should be in the range 10^{-6}–10^{-8} cm^2/s, whereas if particle diffusion is the rate-determining step, then the D_i value should be in the range 10^{-11}–10^{-13} cm^2/s [49]. The D_i values obtained from this work are in the range 10^{-6}–10^{-8} cm^2/s, confirming that the slowest step in HA adsorption on the MIPs is film diffusion.

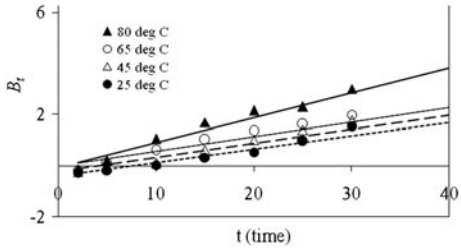

Fig. 12. Boyd kinetic model for for HA removal from peat water at different temperatures (volume 50 mL, dosage 0.5 g, pH 4.02, particle size 75 μm, and shaking speed 100 rpm).

Table 6
The Boyd kinetic model parameters for HA adsorption from peat water using MIPs

Temperature (°C)	R^2	D_i ($\times 10^{-8}$ cm^2/s)
25	0.945	7.42
45	0.905	7.84
65	0.900	7.99
80	0.974	13.84

3.8. Thermodynamic studies

Thermodynamic considerations of an adsorption process are necessary to conclude whether the process is spontaneous or not. The experimental data obtained at different temperatures were used in calculating the thermodynamic parameters such as Gibbs free energy change (ΔG°), enthalpy change (ΔH°), and entropy change (ΔS°). The thermodynamic parameters were determined using the following equations:

$$\Delta G^\circ = -RT \ln b \tag{12}$$

where

$$\ln b = \frac{\Delta S^\circ}{R} - \frac{\Delta H^\circ}{RT} \tag{13}$$

where R (8.314 J/mol K) is the gas constant, T (K) is the absolute temperature, and K_b (L/mg) is the Langmuir isotherm constant. The value enthalpy (ΔH°) and entropy (ΔS°) were calculated from the slope and intercept of the plot of ln K_b vs 1/T. The results are listed in Table 7.

The positive values of Gibbs free energy (ΔG°) at all temperatures showed that the removal process was non-spontaneous. The decrease of the Gibbs free energy (ΔG°) from 1.17 to 3.71 kJ/mol with increase temperature from 25 to 80°C indicated that the presence of an energy barrier at low temperature [50]. The value of ΔG° becomes more negative with the increase of temperature, which indicates that the reaction is more favorable at high temperatures.

The positive ΔH° values obtained indicated that the sorption process was endothermic in nature. Generally, the enthalpy change (ΔH°) for physical sorption is in the range 2.1–20.9 kJ/mol and chemical sorption is in the range 80–200 kJ/mol [34]. Since the value of ΔH° observed in the system is 16.17 kJ/mol, this process can be considered as physisorption. The positive value of entropy change (ΔS°) indicates the increased randomness at the solid–solution interface during the adsorption of HA onto MIPs [34,41,42,50].

The other thermodynamic parameter is activation energy (E_a). The Arrhenius equation was applied to evaluate the E_a of the adsorption process:

$$\ln k = \ln A - \frac{Ea}{RT} \tag{14}$$

where k is rate constant of pseudo-second-order kinetic model (g/mg min), E_a is the activation energy (kJ/mol), A the Arrhenius factor, R the gas constant (8.314 J/mol K), and T is the solution absolute temperature (K). The linear plot of ln k vs. $1/T$ gives a straight line with slope $-E_a/R$. The magnitude of E_a gives an opinion about the adsorption mechanism [41,42,50]. Physical adsorption typically has activation energy of 5–40 kJ/mol and chemical adsorption has activation energy of 40–800 kJ/mol [41,42,50]. The activation energy obtained in this study is 18.62 kJ/mol (Table 7), indicating that HA adsorption

Table 7
Thermodynamic parameters for HA adsorption from peat water using MIPs

Temperature (°C)	b (L/mg)	ΔG° (kJ/mol)	ΔH° (kJ/mol)	ΔS° (kJ/mol)	E_a (kJ/mol)
25	0.224	3.706	16.17	42.70	18.62
45	0.422	2.281			
65	0.538	1.742			
80	0.675	1.170			

onto the MIPs corresponds to physisorption. The positive value of E_a suggests that an increase in temperature favors the adsorption of HA on MIPs and the adsorption process is endothermic in nature [34].

4. Conclusions

The MIPs can be effectively used as adsorbent for the adsorption of HA from peat water. The HA adsorption percentage increases with an increase in the adsorbent dosages and temperatures. The HA adsorption percentage decreases with increasing peat water pH from 2 to 12. The equilibrium adsorption data of HA on the MIPs fit the Langmuir isotherm model better than both Freundlich and Sips isotherm models. Based on the Langmuir isotherm model, the maximum monolayer adsorption capacity is 45.45 mg/g. The result of the kinetic study shows that the adsorption of HA onto the MIPs could be described by the pseudo-second-order kinetic models with a rate constant in the range of 0.034–0.115 g/mg min. The adsorption process was found to be controlled by both film and pore diffusion, with film diffusion at the earlier stages followed by pore diffusion at the later stages. Analysis of adsorption data using a Boyd kinetic plot confirmed that film diffusion is the rate-determining step in the sorption process with the effective diffusion coefficient in the range of 7.42×10^{-8}–13.84×10^{-8} cm^2/s. Thermodynamic parameters data indicated that the HA adsorption process was non-spontaneous and endothermic under the experimental conditions, with the Gibbs free energy (ΔG°) in the range of 3.71–1.17 kJ/mol, enthalpy (ΔH°) and entropy (ΔS°) of 16.17 kJ/mol and 42.70 J/mol, respectively. The results of this study show that the MIPs are a promising adsorbent for removing HA from peat water.

Acknowledgments

The authors are very grateful to Institut Teknologi Bandung for their financial support through Riset KK dan Inovasi ITB 2013. The authors also wish to thank to Mr Andhika Nugraha for English correction of the manuscript.

References

[1] B. Libecki, J. Dziejowski, Optimization of humic acids coagulation with aluminum and iron(III) salts, Pol. J. Environ. Stud. 17(3) (2008) 397–403.
[2] S. Park, T. Yoon, Effects of iron species and inert minerals on coagulation and direct filtration for humic acid removal, Desalination 239 (2009) 146–158.
[3] C. Sun, Q. Yue, B. Gao, R. Mu, J. Liu, Y. Zhao, Z. Yang, W. Xu, Effect of pH and shear force on flocs characteristics for humic acid removal using polyferric aluminum chloride organic polymer dual-coagulants, Desalination 281 (2011) 243–247.
[4] J.C. Rojas, J. Pérez, G. Garralón, F. Plaza, B. Moreno, M.A. Gómez, Humic acids removal by aerated spiral-wound ultrafiltration membrane combined with coagulation–hydraulic flocculation, Desalination 266 (2011) 128–133.
[5] D. Ghernaout, B. Ghernaout, A. Saiba, A. Boucherit, A. Kellil, Removal of humic acids by continuous electromagnetic treatment followed by electrocoagulation in batch using aluminium electrodes, Desalination 239 (2009) 295–308.
[6] C.S. Uyguner, S.A. Suphandag, A. Kerc, M. Bekbolet, Evaluation of adsorption and coagulation characteristics of humic acids preceded by alternative advanced oxidation techniques, Desalination 210 (2007) 183–193.
[7] D. Sonea, R. Pode, F. Manea, C. Ratiu, C. Lazau, I. Grozescu, G. Burtica, The comparative assessment of photolysis, sorption and photocatalysis processes to humic acids removal from water, Chem. Bull. "POLITEHNICA" Univ. (Timisoara) 55(69) (2010) 148–151.
[8] F.X. Simon, E. Rudé, J. Llorens, S. Baig, Study on the removal of biodegradable NOM from seawater using biofiltration, Desalination 316 (2013) 8–16.
[9] N.A.A. Hamid, A.F. Ismail, T. Matsuura, A.W. Zularisam, W.J. Lau, E. Yuliwati, M.S. Abdullah, Morphological and separation performance study of polysulfone/titanium dioxide (PSF/TiO_2) ultrafiltration membranes for humic acid removal, Desalination 273 (2011) 85–92.
[10] K.S. Katsoufidou, D.C. Sioutopoulos, S.G. Yiantsios, A.J. Karabelas, UF membrane fouling by mixtures of humic acids and sodium alginate: Fouling mechanisms and reversibility, Desalination 264 (2010) 220–227.
[11] J. Lowe, M.M. Hossain, Application of ultrafiltration membranes for removal of humic acid from drinking water, Desalination 218 (2008) 343–354.
[12] M.A.F. Ferro-García, J.R. Rivera-Utrilla, I.B. Bautista-Toledo, C.M. Moreno-Castilla, Adsorption of humic substances on activated carbon from aqueous solutions and their effect on the removal of Cr(III) ions, Langmuir 14 (1998) 1880–1886.
[13] A.A.M. Daifullah, B.S. Girgis, H.M.H. Gad, A study of the factors affecting the removal of humic acid by activated carbon prepared from biomass material, Colloids Surf., A 235 (2004) 1–10.
[14] S. Maghsoodloo, B. Noroozi, A.K. Haghi, G.A. Sorial, Consequence of chitosan treating on the adsorption of humic acid by granular activated carbon, J. Hazard. Mater. 191 (2011) 380–387.
[15] M.A. Zulfikar, E. Novita, R. Hertadi, S.D. Djajanti, Removal of humic acid from peat water using untreated powdered eggshell as a low cost adsorbent, Int. J. Environ. Sci. Technol. 10 (2013) 1357–1366.
[16] X. Peng, Z. Luan, F. Chen, B. Tian, Z. Jia, Adsorption of humic acid onto pillared bentonite, Desalination 174 (2005) 135–143.
[17] M. Salman, B. El-Eswad, F. Khalili, Adsorption of humic acid on bentonite, Appl. Clay Sci. 38 (2008) 51–56.
[18] D. Doulia, C. Leodopoulos, K. Gimouhopoulos, F. Rigas, Adsorption of humic acid on acid-activated

Greek bentonite, J. Colloid Interface Sci. 340 (2009) 131–141.
[19] L. Zhang, L. Luo, S. Zhang, Integrated investigations on the adsorption mechanisms of fulvic and humic acids on three clay minerals, Colloids Surf., A. 406 (2012) 84–90.
[20] W.S.W. Ngah, A. Musa, Adsorption of humic acid onto chitin and chitosan, J. Appl. Polym. Sci. 69 (1998) 2305–2310.
[21] W.S. Wan Ngah, M.A.K.M. Hanafiah, S.S. Yong, Adsorption of humic acid from aqueous solutions on crosslinked chitosan-epichlorohydrin beads: Kinetics and isotherm studies, Colloids Surf., B. 65 (2008) 18–24.
[22] M.Y. Chang, R.S. Juang, Adsorption of tannic acid, humic acid, and dyes from water using the composite of chitosan and activated clay, J. Colloid Interface Sci. 278 (2004) 18–25.
[23] X. Zhang, R. Bai, Mechanisms and kinetics of humic acid adsorption onto chitosan-coated granules, J. Colloid Interface Sci. 264 (2003) 30–38.
[24] W.S.W. Ngah, S. Fatinathan, N.A. Yosop, Isotherm and kinetic studies on the adsorption of humic acid onto chitosan-H_2SO_4 beads, Desalination 272 (2011) 293–300.
[25] L. Liang, L. Luo, S. Zhang, Adsorption and desorption of humic and fulvic acids on SiO_2 particles at nano- and micro-scales, Colloids Surf., A. 384 (2011) 126–130.
[26] S. Wang, Z.H. Zhu, Humic acid adsorption on fly ash and its derived unburned carbon, J. Colloid Interface Sci. 315 (2007) 41–46.
[27] S. Wang, T. Terdkiatburana, M.O. Tadé, Single and co-adsorption of heavy metals and humic acid on fly ash, Sep. Purif. Technol. 58 (2008) 353–358.
[28] S. Wang, Q. Ma, Z.H. Zhu, Characteristics of coal fly ash and adsorption application, Fuel 87 (2008) 3469–3473.
[29] M.S. Gasser, H.T. Mohsen, H.F. Aly, Humic acid adsorption onto Mg/Fe layered double hydroxide, Colloids Surf., A 331 (2008) 195–201.
[30] L. Zhao, F. Luo, J.M. Wasikiewicz, H. Mitomo, N. Nagasawa, T. Yagi, M. Tamada, F. Yoshii, Adsorption of humic acid from aqueous solution onto irradiation crosslinked carboxymethylchitosan, Bioresour. Technol. 99 (2008) 1911–1917.
[31] Q. Tao, Z. Xu, J. Wang, F. Liu, H. Wan, S. Zheng, Adsorption of humic acid to aminopropyl functionalized SBA-15, Microporous Mesoporous Mater. 131 (2010) 177–185.
[32] A. Imyim, E. Prapalimrungsi, Humic acids removal from water by aminopropyl functionalized rice husk ash, J. Hazard. Mater. 184 (2010) 775–781.
[33] J. Wang, X. Han, H. Ma, Y. Ji, L. Bi, Adsorptive removal of humic acid from aqueous solution on polyaniline/attapulgite composite, Chem. Eng. J. 173 (2011) 171–177.
[34] J. Lin, Y. Zhan, Adsorption of humic acid from aqueous solution onto unmodified and surfactant-modified chitosan/zeolite composites, Chem. Eng. J. 200–202 (2012) 202–213.
[35] J. He, R. Lv, J. Zhu, K. Lu, Selective solid-phase extraction of dibutyl phthalate from soybean milk using molecular imprinted polymers, Anal. Chim. Acta 661 (2010) 215–221.
[36] J. Yao, X. Li, W. Qin, Computational design and synthesis of molecular imprinted polymers with high selectivity for removal of aniline from contaminated water, Anal. Chim. Acta 610 (2008) 282–288.
[37] W. Zhao, N. Sheng, R. Zhu, F. Wei, Z. Cai, M. Zhai, S. Du, Q. Hu, Preparation of dummy template imprinted polymers at surface of silica microparticles for the selective extraction of trace bisphenol A from water samples, J. Hazard. Mater. 179 (2010) 223–229.
[38] L.E. Gómez-Pineda, G.E. Pina-Luis, Á. Cuán, J.A. García-Calzón, M.E. Díaz-García, Physico-chemical characterization of flavonol molecularly imprinted polymers, React. Funct. Polym. 71 (2011) 402–408.
[39] E. Demirbas, N. Dizge, M.T. Sulak, M. Kobya, Adsorption kinetics and equilibrium of copper from aqueous solutions using hazelnut shell activated carbon, Chem. Eng. J. 148 (2009) 480–487.
[40] I.G. Altındağ, A. Dinçer, S. Becerik, A. Eser, T. Aydemir, Poly(methyl methacrylate-ethylene glycol dimethacrylate) copolymer for adsorptive removal of erythrosine dye from aqueous solution, Desalin. Water Treat. 54(6) (2015) 1717–1726, doi: 10.1080/19443994.2014.888015.
[41] J. Fan, W. Cai, J. Yu, Adsorption of N719 dye on anatase TiO2 nanoparticles and nanosheets with exposed (001) facets: Equilibrium, kinetic, and thermodynamic studies, Chem. Asian J. 6 (2011) 2481–2490.
[42] J. Rahchamani, H.Z. Mousavi, M. Behzad, Adsorption of methyl violet from aqueous solution by polyacrylamide as an adsorbent: Isotherm and kinetic studies, Desalination 267 (2011) 256–260.
[43] L. Wang, A. Wang, Adsorption properties of congo red from aqueous solution onto N,O-carboxymethylchitosan, Bioresour. Technol. 99 (2008) 1403–1408.
[44] L. Wang, A. Wang, Adsorption properties of Congo Red from aqueous solution onto surfactant-modified montmorillonite, J. Hazard. Mater. 160 (2008) 173–180.
[45] M.A. Zulfikar, H. Setiyanto, Study of the adsorption kinetics and thermodynamic for the removal of Congo red from aqueous solution using powdered eggshell, Int. J. Chem. Technol. Res. 5(4) (2013) 1671–1678.
[46] M.A. Zulfikar, D. Wahyuningrum, S. Lestari, Adsorption of lignosulfonate compound from aqueous solution onto chitosan-silica beads, Sep. Sci. Technol. 48 (2013) 1391–1401.
[47] M.F. Elkady, A.M. Ibrahim, M.M. Abd, El-Latif, Assessment of the adsorption kinetics, equilibrium and thermodynamic for the potential removal of reactive red dye using chitosan-silica biobeads beads, Desalination 278 (2011) 412–423.
[48] X.J. Hu, J.S. Wang, Y.G. Liu, X. Li, G.M. Zeng, Z.L. Bao, X.X. Zeng, A.W. Chen, F. Long, Adsorption of chromium(VI) by ethylenediamine-modified cross-linked magnetic chitosan resin: Isotherms, kinetics and thermodynamics, J. Hazard. Mater. 185 (2011) 306–314.
[49] W.S.W. Ngah, M.A.K.M. Hanafiah, Biosorption of copper ions from dilute aqueous solutions on base treated rubber (*Hevea brasiliensis*) leaves powder: Kinetics, isotherm, and biosorption mechanisms, J. Environ. Sci. 20 (2008) 1168–1176.
[50] W. Wang, B. Zheng, Z. Deng, Z. Feng, L. Fu, Kinetics and equilibriums for adsorption of poly(vinyl alcohol) from aqueous solution onto natural bentonite, Chem. Eng. J. 214 (2013) 343–354.